Biophysical Journal
Article

Biophysical Society

Effects of membrane viscoelasticity on the red blood cell dynamics in a microcapillary

Ali Gürbüz,[1,*] On Shun Pak,[1] Michael Taylor,[1] Mettupalayam V. Sivaselvan,[2] and Frederick Sachs[3]
[1]Department of Mechanical Engineering, Santa Clara University, Santa Clara, California; [2]Department of Civil, Structural and Environmental Engineering, University at Buffalo, Buffalo, New York; and [3]Department of Physiology and Biophysics, University at Buffalo, Buffalo, New York

ABSTRACT The mechanical properties of red blood cells (RBCs) play key roles in their biological functions in microcirculation. In particular, RBCs must deform significantly to travel through microcapillaries with sizes comparable with or even smaller than their own. Although the dynamics of RBCs in microcapillaries have received considerable attention, the effect of membrane viscoelasticity has been largely overlooked. In this work, we present a computational study based on the boundary integral method and thin-shell mechanics to examine how membrane viscoelasticity influences the dynamics of RBCs flowing through straight and constricted microcapillaries. Our results reveal that the cell with a viscoelastic membrane undergoes substantially different motion and deformation compared with results based on a purely elastic membrane model. Comparisons with experimental data also suggest the importance of accounting for membrane viscoelasticity to properly capture the transient dynamics of an RBC flowing through a microcapillary. Taken together, these findings demonstrate the significant effects of membrane viscoelasticity on RBC dynamics in different microcapillary environments. The computational framework also lays the groundwork for more accurate quantitative modeling of the mechanical response of RBCs in their mechanotransduction process in subsequent investigations.

SIGNIFICANCE There has been substantial interest in the critical roles the dynamics of red blood cells (RBCs) play in microcirculation and mechanotransduction. However, the effect of membrane viscoelasticity has been largely overlooked in previous studies. In this work, we present a computational framework to probe the significance of membrane viscoelasticity on the dynamics of RBCs in microcapillaries. Through two physiologically relevant flow setups, our results demonstrate how membrane viscoelasticity can significantly influence the motion and deformation of RBCs traveling through different microcapillary environments. These findings help establish the importance of accounting for membrane viscoelasticity in quantitative modeling of RBC dynamics, laying the foundation for more accurate biophysical models to understand the mechanotransduction of RBCs in future studies.

INTRODUCTION

Blood is a complex fluid and its composition consists of plasma fluid and cellular elements such as platelets, white blood cells, and red blood cells (RBCs). The high concentration of RBCs governs the rheological and transport properties of blood in the microcirculation (1,2). The RBC membrane is a thin viscoelastic envelope, and its biconcave geometric shape allows it to deform and squeeze through the microcapillaries (3). It is mainly composed of a lipid bilayer, cytoskeleton, and transmembrane proteins. The cytoskeleton binds to the cytoplasm side of the lipid bilayer and supports its structural shape. It is made mainly of triangular spectrin proteins, and it is postulated that these spectrin tetramers are responsible for the viscoelastic properties of the RBC membrane (4–7).

Although experimental studies have observed the viscoelastic behavior of the RBC membrane (8–12), only recently, in numerical studies, has there been increased emphasis on the significant effects of the membrane viscoelasticity on the motion and deformation of the RBCs. For example, it has been demonstrated that the magnitude and rate of RBC deformation reduce with increasing membrane viscosity. However, these studies are limited to the dynamics of spherical capsules and biconcave RBC under shear flow or pull and relaxation type investigations in an unbounded domain (13–19). Previous studies have shed light on the dynamics of capsules, vesicles, and RBCs in

Submitted August 31, 2022, and accepted for publication January 9, 2023.
*Correspondence: agurbuz@scu.edu
Editor: Padmini Rangamani.
https://doi.org/10.1016/j.bpj.2023.01.010

straight (20–23) and constricted (6,24) microcapillaries. However, few studies have assessed the significance of membrane viscoelasticity on the long- and short-time-scale transient deformation of an RBC in these configurations.

Previous numerical studies on RBC motion and deformation at the cellular level in a confined domain have only considered the effects of the purely elastic components of membrane mechanics, which consist of dilatational, shear, and bending forces (25–28). Some of these studies have attempted to capture the viscoelastic behavior of the RBC in unbounded and confined domains by considering a purely elastic membrane model with an exceedingly high intracellular fluid viscosity compared with the dynamic viscosity of the extracellular fluid (16,29,30). The ratio of the viscosities of the intracellular fluid to the extracellular fluid is called the viscosity ratio. In the unbounded domain, it has been shown that the assumption of a high viscosity ratio qualitatively captures the effects of membrane viscoelasticity but yields quantitatively different results (16,17,31). However, what is not yet understood is the degree to which the viscosity ratio captures the behavior of the membrane viscosity in a microcapillary under the influence of pressure-driven flows.

In this study, we aim to fill these gaps in the literature by investigating the significance of membrane viscoelasticity on the mode, magnitude, and rate of motion and deformation of an RBC flowing in straight and constricted microcapillaries under pressure-driven flows. In addition, we assess to what extent the purely elastic membrane model with high viscosity ratio captures the effects of the membrane viscoelasticity on RBC dynamics in a straight microcapillary and examine whether the high-viscosity-ratio assumption misses the important physics of the shape transition of the RBC deformation.

We used the boundary integral representation of Stokes flow to describe the hydrodynamics of the intracellular and extracellular fluids of an RBC inside a rigid microcapillary. The advantage of this representation is that the features of fluid-structure interaction problem are built into the boundary integral formulation. The effects of the hydrodynamical stresses of the intra- and extracellular fluids on the cell membrane are balanced by the membrane internal forces. We use thin-shell theory with Kirchhoff-Love kinematics to compute the membrane internal forces due to the deformation caused by the fluid stresses. The elastic component of in-plane stresses is described by Skalak's constitutive equation, and the viscous component of the in-plane stresses is described by Maxwell's dynamic constitutive equation. The combination of these in-plane stresses yields what is called the standard linear solid model. The linear isotropic form of the Helfrich model is used to compute the bending forces.

We study the impact of the membrane viscosity and the viscosity ratio on the long-time-scale deformation of the RBC in a rigid cylindrical straight microcapillary under the influence of pressure-gradient fluid flow. We analyze the shape transition, magnitude, and rate of the RBC membrane deformation up to a steady-state parachute shape with increasing membrane viscosity (from 0 to 1 μN.m/s) and viscosity ratio (from 5 to 50) of a purely elastic membrane model. We also study the effects of the membrane viscosity on the short-time-scale deformation and motion of an RBC while flowing through a constriction under the pressure-driven flow field with increasing membrane viscosity (from 0 to 1 μN.m/s).

The novelty of this study is that it provides important results that demonstrate the effects of the membrane viscoelasticity on the long- and short-timescale deformation of the RBC while flowing inside a straight and constricted microcapillary, respectively. In addition, this study offers insight into the physical mechanisms underlying the similar effects of the membrane viscosity and viscosity ratio on the deformation of the RBC in a straight microcapillary.

METHODS

Intra- and extracellular flows

We assume that Stokes flow describes the hydrodynamics of the intra- and extracellular fluids of an RBC inside a rigid microcapillary. In this study, Stokes flow is represented in the form of boundary integral equations (BIEs) that make use of the fundamental solution of velocity $\mathrm{G}(\mathbf{x}_0,\mathbf{x})$ and traction $\mathrm{K}(\mathbf{x}_0,\mathbf{x})$ of the Stokes equation (32,33) in the following form:

$$\mathrm{G}(\mathbf{x}_0,\mathbf{x}) = \frac{1}{\|\mathbf{r}\|}(I+\hat{\mathbf{r}}\hat{\mathbf{r}}^{\top}),\ \mathrm{K}(\mathbf{x}_0,\mathbf{x}) = \frac{6}{\|\mathbf{r}\|^2}(\hat{\mathbf{r}}^{\top}\mathbf{n})\hat{\mathbf{r}}\hat{\mathbf{r}}^{\top}, \tag{1}$$

where $\mathbf{r} = \mathbf{r}(\mathbf{x}_0,\mathbf{x}) = \mathbf{x}_0 - \mathbf{x}$, the corresponding unit vector $\hat{\mathbf{r}} = \mathbf{r}/\|\mathbf{r}\|$, $\mathbf{x}$ denotes the field point, and $\mathbf{x}_0$ denotes the target point. This approach is widely used in the literature to formulate the motion and deformation of RBC, capsules, and droplets in unbounded and confined domains (34–38). The system of BIEs is provided to describe unknown variables; the membrane velocity field ($\mathbf{u}^{\mathrm{C}}$) on the cell membrane (Γ_{C}) and the velocity ($\mathbf{u}^{\mathrm{E}}$) and traction ($\mathbf{t}^{\mathrm{E}}$) fields on the microcapillary boundary (Γ_{E}) by the following two weakly singular BIEs:

$$\begin{aligned}
&\mathbf{u}^{\mathrm{C}}(\mathbf{x}_0)+\frac{\lambda-1}{8\pi}\int_{\Gamma_{\mathrm{C}}}\mathrm{K}(\mathbf{x}_0,\mathbf{x})(\mathbf{u}^{\mathrm{C}}(\mathbf{x})-\mathbf{u}^{\mathrm{C}}(\mathbf{x}_0))\mathrm{d}\Gamma(\mathbf{x})\\
&-\mathbf{u}^{\mathrm{E}}(\mathbf{x}_\perp)+\frac{1}{8\pi}\int_{\Gamma_{\mathrm{E}}}\mathrm{K}(\mathbf{x}_0,\mathbf{x})\big(\mathbf{u}^{\mathrm{E}}(\mathbf{x})-\mathbf{u}^{\mathrm{E}}(\mathbf{x}_\perp)\big)\mathrm{d}\Gamma(\mathbf{x})\\
&\quad=-\frac{1}{8\pi\mu}\int_{\Gamma_{\mathrm{C}}}\mathrm{G}(\mathbf{x}_0,\mathbf{x})\mathbf{f}^{\mathrm{C}}(\mathbf{x})\mathrm{d}\Gamma(\mathbf{x})\\
&\quad+\frac{1}{8\pi\mu}\int_{\Gamma_{\mathrm{E}}}\mathrm{G}(\mathbf{x}_0,\mathbf{x})\mathbf{t}^{\mathrm{E}}(\mathbf{x})\mathrm{d}\Gamma(\mathbf{x}),\ \mathbf{x}_0\in\Gamma_{\mathrm{C}},
\end{aligned} \tag{2}$$

$$\begin{aligned}
&\frac{\lambda-1}{8\pi}\int_{\Gamma_{\mathrm{C}}}\mathrm{K}(\mathbf{x}_0,\mathbf{x})(\mathbf{u}^{\mathrm{C}}(\mathbf{x})-\mathbf{u}^{\mathrm{C}}(\mathbf{x}_\perp))\mathrm{d}\Gamma(\mathbf{x})\\
&+\frac{1}{8\pi}\int_{\Gamma_{\mathrm{E}}}\mathrm{K}(\mathbf{x}_0,\mathbf{x})\big(\mathbf{u}^{\mathrm{E}}(\mathbf{x})-\mathbf{u}^{\mathrm{E}}(\mathbf{x}_0)\big)\mathrm{d}\Gamma(\mathbf{x})\\
&\quad=-\frac{1}{8\pi\mu}\int_{\Gamma_{\mathrm{C}}}\mathrm{G}(\mathbf{x}_0,\mathbf{x})\mathbf{f}^{\mathrm{C}}(\mathbf{x})\mathrm{d}\Gamma(\mathbf{x})\\
&+\frac{1}{8\pi\mu}\int_{\Gamma_{\mathrm{E}}}\mathrm{G}(\mathbf{x}_0,\mathbf{x})\mathbf{t}^{\mathrm{E}}(\mathbf{x})\mathrm{d}\Gamma(\mathbf{x}),\ \mathbf{x}_0\in\Gamma_{\mathrm{E}},
\end{aligned} \tag{3}$$

where $\mathbf{x}_\perp$ is the closest point to the target point on Γ_E in Eq. 2 when $\mathbf{x}_0 \in \Gamma_C$ and the closest point to the target point on Γ_C in Eq. 3 when $\mathbf{x}_0 \in \Gamma_E$. The proposed BIEs not only consider the interacting surfaces of the cell membrane with the microcapillary sidewalls but also account for the nearly singular nature of the integral equations, using the singularity subtraction technique (5,39–41), where the cell membrane is in close proximity to the microcapillary boundary. This reduction of the strongly and nearly singular form of integrals to a weakly singular form is a major advantage of the formulation. The Galerkin spectral boundary integral method is used for the solution of membrane velocity using spherical harmonic basis functions (27,42,43), and the boundary element method is used for the solution of traction and velocity fields on a discretized microcapillary (44–46). The coupled system of BIEs is solved iteratively and an adaptive time-stepping scheme is used for time integration to compute the new position of the RBC after solving for the membrane velocity $\mathbf{u}^C$. A summary of the numerical algorithm is provided in section S1 in the supporting material. We also direct the interested reader to (47) for a detailed description of the BIE formulation for the dynamics of RBC in bounded and unbounded domains and its numerical solution schemes. The membrane force field $\mathbf{f}^C$ enters the BIEs (Eqs. 2 and 3) through its balance with the hydrodynamic stresses of the fluid across the cell membrane (35,38,48) as

$$\mathbf{f}^C(\mathbf{x}) = [\boldsymbol{T}_{EXT}(\mathbf{x}) - \boldsymbol{T}_{INT}(\mathbf{x})]\mathbf{n}_{INT}(\mathbf{x}), \quad (4)$$

building the fluid-structure interaction into the boundary integral formulation. Here, stresses due to extracellular and intracellular fluid are denoted as $\boldsymbol{T}_{EXT}$ and $\boldsymbol{T}_{INT}$ on the cell membrane, and $\mathbf{n}_{INT}(\mathbf{x})$ denotes the unit normal vector that points outward from the intracellular fluid domain Ω_{INT} as shown in Fig. 1.

Membrane mechanics

The RBC membrane is a thin shell-like envelope that separates intracellular fluid from extracellular fluid. It comprises a lipid bilayer and a cytoskeleton network that is made up of spectrin proteins that underlie the bilayer. Transmembrane proteins are embedded in this envelope as a gateway to regulate ion and water flows (49–51). This composite membrane structure allows the cell to resist hydrodynamic forces by developing internal bending and in-plane viscoelastic stresses without changing the surface area. The large surface area to volume ratio of the biconcave shape allows the RBC to deform and squeeze through a constriction without changing the surface area (52–54). There are computational models that account for lipid bilayer and cytoskeletal interactions in an RBC (7,51,55,56). A recent model has also examined the coupled in-plane viscous flow of lipids, transmembrane protein diffusion, and elastic deformation of lipid bilayer membrane (57).

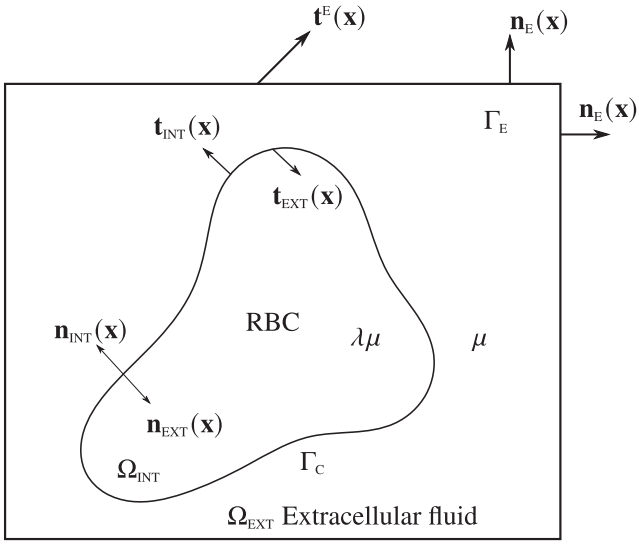

FIGURE 1 An RBC flow in a microcapillary. RBC motion is confined by the microcapillary boundary (Γ_E) where the traction field ($\mathbf{t}^E$) acts on and the unit normal vector ($\mathbf{n}_E$) points outward from the extracellular fluid domain (Ω_{EXT}). Note that this Ω_{EXT} fluid domain is not only bounded by the Γ_E but also by the cell membrane (Γ_C), which contains the extracellular fluid of viscosity μ. The intracellular fluid of viscosity $\lambda\mu$ is enclosed by the Γ_C in the fluid domain Ω_{INT}. The traction fields ($\mathbf{t}_{INT} = \boldsymbol{T}_{INT}\mathbf{n}_{INT}$ and $\mathbf{t}_{EXT} = \boldsymbol{T}_{EXT}\mathbf{n}_{EXT}$) are defined by the stresses due to the intra and extracellular fluid ($\boldsymbol{T}_{INT}$ and $\boldsymbol{T}_{EXT}$) on the Γ_C where the unit normal vectors ($\mathbf{n}_{INT}$ and $\mathbf{n}_{EXT}$) point outward from fluid domains (Ω_{INT} and Ω_{EXT}), respectively.

Although the effects of the cytoskeletal network and transmembrane proteins are assumed to be embedded in some measured values of elastic and viscoelastic properties of the RBC membrane, we do not model these effects explicitly in this work. We describe membrane forces $\mathbf{f}^C$ in the framework of thin-shell theory with Kirchhoff-Love kinematics (36,37,58–62). Our membrane mechanics take into account the viscoelasticity of the in-plane membrane stresses using the standard linear solid model, which is central to the objectives of this study. This approach was chosen to account for creep and relaxation behaviors. The elastic component of in-plane stress is described by Skalak's constitutive equation, and the viscous component by the Maxwell model. Bending stresses are computed using the Helfrich model in linear isotropic form. The detailed mathematical formulation for the RBC membrane mechanics is provided in (47). We provide a brief summary in the following subsections.

Constitutive equations

In-plane stresses. In recent years, there has been increased emphasis on the effects of membrane viscoelasticity on the dynamics of RBCs (14–16,63–65). In-plane membrane stresses consist of the elastic stress component $\boldsymbol{\sigma}^E$ and the viscoelastic stress component $\boldsymbol{\sigma}^V$ such as $\boldsymbol{\sigma} = \boldsymbol{\sigma}^E + \boldsymbol{\sigma}^V$.

Skalak model. The Skalak strain energy function tailored for the RBC membrane has the following form (36,66,67):

$$W = \frac{E_S}{4}\left(\frac{1}{2}\mathbb{I}_1^2 + \mathbb{I}_1 - \mathbb{I}_2\right) + \frac{E_D}{8}\mathbb{I}_2^2, \quad (5)$$

where E_S and E_D denote, respectively, the shear and dilatation modulus, and the first and second strain invariants are given as $\mathbb{I}_1 = 2\mathrm{tr}\boldsymbol{\varepsilon}$ and $\mathbb{I}_2 = 2\mathrm{tr}\,\boldsymbol{\varepsilon} + 4\det\boldsymbol{\varepsilon}$, respectively. The surface strain tensor $\boldsymbol{\varepsilon}$ is defined as the change in the metric tensor due to surface deformation $\boldsymbol{\varepsilon} = \frac{1}{2}\mathbf{A}^{-1}(\mathbf{a} - \mathbf{A})$, where the metric tensor is defined using the surface gradient of position vectors in the undeformed ($\boldsymbol{\Xi}$) and deformed ($\boldsymbol{\xi}$) configuration as $\mathbf{A} = \nabla\boldsymbol{\Xi}^\top\nabla\boldsymbol{\Xi}$ and $\mathbf{a} = \nabla\boldsymbol{\xi}^\top\nabla\boldsymbol{\xi}$, respectively. Elastic in-plane membrane stresses can be written as

$$\boldsymbol{\sigma}^E = \frac{E_D}{2}\mathbb{I}_2(I + 2\boldsymbol{\epsilon}) + \frac{E_S}{2}(\mathbb{I}_1 I - 2\boldsymbol{\epsilon}), \quad (6)$$

where $\boldsymbol{\epsilon} = \boldsymbol{\varepsilon}^{-\top}\det\boldsymbol{\varepsilon}$.

Viscoelastic model. The Maxwell model is an ordinary differential equation for viscoelastic stresses of the membrane $\boldsymbol{\sigma}^V$ with constant coefficients given as (68,69)

$$\dot{\boldsymbol{\sigma}}^V + \frac{\boldsymbol{\sigma}^V}{2\tau} = k'\dot{\boldsymbol{\varepsilon}}, \quad (7)$$

where $\tau = \mu_m/k'$ denotes the relaxation time of the Maxwell element, with μ_m being the membrane viscosity and k' being the artificial spring modulus. The term $k'\dot{\boldsymbol{\varepsilon}}$ is the forcing function and an overdot denotes differentiation with respect to time.

An approach based on the finite difference method is provided (70,71) for viscoelastic membrane stresses. Using this approach by applying the central finite difference approximation, from $t - \Delta t$ to t, to the time rate terms

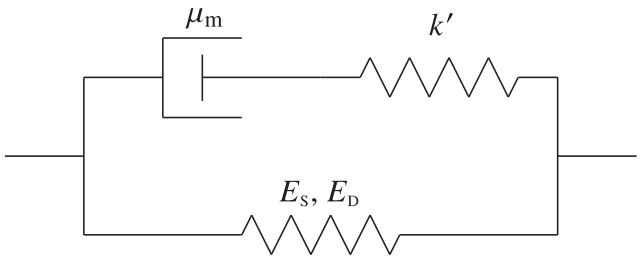

FIGURE 2 A conceptual representation of the standard linear solid model (13,16,68,70) for modeling the viscoelastic in-plane stresses.

in Eq. 7 and taking the average of the term $\boldsymbol{\sigma}^V$ in $\left(t-\frac{\Delta t}{2}\right)$ leads to the following form of a constitutive equation for the computation of the viscoelastic in-plane stresses $\boldsymbol{\sigma}^V$:

$$\boldsymbol{\sigma}^V(t_i) = \frac{4\tau - \Delta t}{4\tau + \Delta t}\boldsymbol{\sigma}^V(t_{i-1}) + \frac{4\mu_m}{4\tau + \Delta t}[\boldsymbol{\varepsilon}(t_i) - \boldsymbol{\varepsilon}(t_{i-1})]^\top. \tag{8}$$

Fig. 2 illustrates a conceptual representation of the membrane mechanics in the standard linear solid model (13,16,68,70): the dashpot element μ_m and the artificial spring k' in series combine to form the Maxwell viscoelastic element (Eq. 7), which integrates with the elastic element given by Skalak's model in parallel (Eq. 6) to form the standard linear solid model for the in-plane stresses.

Helfrich model. The bending stresses in the cell membrane are computed using the Helfrich constitutive equation in linear isotropic form (72,73) as follows:

$$\mathbf{m} = E_B\boldsymbol{\kappa}^\top, \tag{9}$$

where E_B denotes the bending modulus. The change in the curvature tensor field is $\boldsymbol{\kappa} = \mathbf{A}^{-1}(\mathbf{b}-\mathbf{B})$ and the curvature tensors are defined using the gradient of the unit normal vector in the reference and deformed configurations ($\mathbf{N}$ and $\mathbf{n}$) respectively as $\mathbf{B} = \nabla\mathbf{N}^\top\nabla\boldsymbol{\Xi}$ and $\mathbf{b} = \nabla\mathbf{n}^\top\nabla\boldsymbol{\xi}$.

Membrane force field

We consider the variation of the strain energy functional $\Pi[\boldsymbol{\xi}]$ under small deformations $\delta\boldsymbol{\xi}$ to derive the membrane force field $\mathbf{f}^C$ in the deformed configuration. These infinitesimal deformations have to satisfy the Kirchhoff-Love kinematics in the sense that the straight lines normal to the undeformed configuration remain straight and normal in the deformed configuration (74). The strain energy functional can be obtained by integrating the strain energy density function $\Psi(\boldsymbol{\varepsilon},\boldsymbol{\kappa})$ (per unit area of the reference configuration) over the cell configuration in the spherical coordinate system,

$$\Pi[\boldsymbol{\xi}] = \int_0^{2\pi}\int_0^{\pi}\Psi(\boldsymbol{\varepsilon},\boldsymbol{\kappa})J_{\boldsymbol{\Xi}}\mathrm{d}\theta\mathrm{d}\varphi, \tag{10}$$

where the Jacobian determinant of the mapping from the parent geometry to the undeformed and deformed configurations are, respectively, denoted by $J_{\boldsymbol{\Xi}} = \|\nabla_\theta\boldsymbol{\Xi}\times\nabla_\varphi\boldsymbol{\Xi}\|$ and $J_{\boldsymbol{\xi}} = \|\nabla_\theta\boldsymbol{\xi}\times\nabla_\varphi\boldsymbol{\xi}\|$. The unit sphere is taken as the parent geometry for the representation of the cell membrane and parameterized by the spherical coordinate system (θ,φ) with $\theta\in[0,\pi]$ being the latitudinal coordinates and $\varphi\in[0,2\pi)$ being the longitudinal coordinates. Note that the in-plane stresses $\boldsymbol{\sigma}$ and bending stresses $\mathbf{m}$ are defined as $\boldsymbol{\sigma} = \partial\Psi/\partial\boldsymbol{\varepsilon}$ and $\mathbf{m} = \partial\Psi/\partial\boldsymbol{\kappa}$ with the density function.

The first variation of the strain energy functional can be expressed as

$$D\Pi[\boldsymbol{\xi}]\cdot\delta\boldsymbol{\xi} = \int_0^{2\pi}\int_0^{\pi}(\boldsymbol{\sigma}\cdot\delta\boldsymbol{\varepsilon} + \mathbf{m}\cdot\delta\boldsymbol{\kappa})J_{\boldsymbol{\Xi}}\mathrm{d}\theta\mathrm{d}\varphi, \tag{11}$$

with a final form given by (47)

$$D\Pi[\boldsymbol{\xi}]\cdot\delta\boldsymbol{\xi} = \int_0^{2\pi}\int_0^{\pi}\mathbf{f}^C(\boldsymbol{\xi})\cdot\delta\boldsymbol{\xi}J_{\boldsymbol{\xi}}\mathrm{d}\theta\mathrm{d}\varphi. \tag{12}$$

In equilibrium, the integrand of Eq. 12 is equal to zero, and we obtain the membrane forces per unit area of the deformed configuration as the surface divergence of the membrane stresses in the form of

$$\mathbf{f}^C(\boldsymbol{\xi}) = -\frac{1}{J_{\boldsymbol{\xi}}}\left[\frac{\partial}{\partial\theta}(\boldsymbol{T}^\theta\sin\theta) + \frac{\partial}{\partial\varphi}(\boldsymbol{T}^\varphi)\right], \tag{13}$$

where the intrinsic components of the membrane stresses are given by

$$\boldsymbol{T}^\theta = \boldsymbol{\sigma}^\theta J_{\boldsymbol{\Xi}} + \mathbf{m}^\theta J_{\boldsymbol{\Xi}} + \mathbf{s}^\theta,\ \boldsymbol{T}^\varphi = \boldsymbol{\sigma}^\varphi J_{\boldsymbol{\Xi}} + \mathbf{m}^\varphi J_{\boldsymbol{\Xi}} + \mathbf{s}^\varphi. \tag{14}$$

Here, the contribution of the elastic and viscoelastic in-plane stress $\boldsymbol{\sigma} = \boldsymbol{\sigma}^E + \boldsymbol{\sigma}^V = \begin{bmatrix}\sigma_\theta^\theta & \sigma_\varphi^\theta\\ \sigma_\theta^\varphi & \sigma_\varphi^\varphi\end{bmatrix}$ to the components of the membrane stress is given by

$$\boldsymbol{\sigma}^\theta = \nabla\boldsymbol{\xi}\mathbf{A}^{-1}\begin{bmatrix}\sigma_\theta^\theta\\ \sigma_\theta^\varphi\end{bmatrix},\ \boldsymbol{\sigma}^\varphi = \nabla\boldsymbol{\xi}\mathbf{A}^{-1}\begin{bmatrix}\sigma_\varphi^\theta\\ \sigma_\varphi^\varphi\end{bmatrix}, \tag{15}$$

where the elastic stress $\boldsymbol{\sigma}^E$ is defined in Eq. 6 and the viscoelastic stress $\boldsymbol{\sigma}^V$ is defined in Eq. 8. The contribution of bending stress $\mathbf{m} = \begin{bmatrix}m_\theta^\theta & m_\varphi^\theta\\ m_\theta^\varphi & m_\varphi^\varphi\end{bmatrix}$ to the components of the membrane stress is given by

$$\mathbf{m}^\theta = \nabla\mathbf{n}\mathbf{A}^{-1}\begin{bmatrix}m_\theta^\theta\\ m_\theta^\varphi\end{bmatrix},\ \mathbf{m}^\varphi = \nabla\mathbf{n}\mathbf{A}^{-1}\begin{bmatrix}m_\varphi^\theta\\ m_\varphi^\varphi\end{bmatrix}, \tag{16}$$

where the bending stress $\mathbf{m}$ is given in Eq. 9. The contributions of the out-of-plane shear stress $\mathbf{s}^\theta$ and $\mathbf{s}^\varphi$ to the components of the membrane stress is given by

$$\mathbf{s}^\theta = \frac{1}{J_{\boldsymbol{\xi}}}(\nabla_\varphi\boldsymbol{\xi}\times\mathbb{P}\boldsymbol{\zeta}),\ \mathbf{s}^\varphi = \frac{1}{J_{\boldsymbol{\xi}}}(\mathbb{P}\boldsymbol{\zeta}\times\nabla_\theta\boldsymbol{\xi}), \tag{17}$$

where $\mathbb{P} = I - \mathbf{n}\mathbf{n}^\top$ is the projection operator and

$$\boldsymbol{\zeta} = -\frac{1}{\sin\theta}\left[\frac{\partial}{\partial\theta}(\mathbf{q}^\theta\sin\theta) + \frac{\partial}{\partial\varphi}\mathbf{q}^\varphi\right] \tag{18}$$

is the surface divergence involving the terms

$$\mathbf{q}^\theta = \nabla\boldsymbol{\xi}\begin{bmatrix}m_\theta^\theta\\ m_\theta^\varphi\end{bmatrix}^\top\mathbf{A}^{-1},\ \mathbf{q}^\varphi = \nabla\boldsymbol{\xi}\begin{bmatrix}m_\varphi^\theta\\ m_\varphi^\varphi\end{bmatrix}^\top\mathbf{A}^{-1}. \tag{19}$$

RESULTS AND DISCUSSION

The aims of this study are to examine and demonstrate the significance of membrane viscosity on RBC dynamics in a microcapillary. We used boundary integral methods to analyze the magnitude, rate, and mode of RBC deformation under pressure-driven flow in a straight and constricted microcapillary. Membrane mechanics in the framework of thin-shell theory has been developed to demonstrate the influence of membrane viscosity on RBC deformation.

We examine the impact of membrane viscosity on RBC deformation in a rigid cylindrical straight microcapillary. To compare the difference of the impact on the membrane deformation between membrane viscosity and intracellular fluid viscosity, we further analyze the purely elastic membrane model with increasing intracellular fluid viscosity. Next, we investigate the effects of membrane viscosity on the motion and deformation of RBC in a constricted microcapillary.

Straight microcapillary

Effects of the membrane viscosity

We consider an RBC flowing through a straight cylindrical rigid microcapillary with a 10 μm diameter filled with extracellular fluid of dynamic viscosity μ. The RBC contains an intracellular fluid with a dynamic viscosity $\lambda\mu$ with λ being the ratio of fluid viscosities of the intra and extracellular fluid. Here, we follow previous studies by assuming $\lambda = 5$ for a healthy RBC (27,48,75); we examine the impact of this assumption in the next subsection. The center line of the cylindrical microcapillary is aligned with the X-axis, and the origin of the coordinate system is set at the centroid of the microcapillary. The initial position of the RBC is at the origin of the coordinate system. Fig. 3 shows the setup of the problem and the initial position and orientation of the RBC.

Deformation of the RBC membrane depends on the key physical and geometric properties of the membrane and the external hydrodynamic system. The physical properties of the red cell membrane are given in Table 1 (15,34,76,77). The viscosity of the membrane μ_m is varied from 0 to 1 μN.m/s to study its effects on the deformation of the red cell membrane while keeping other physical properties constant. The limit of zero membrane viscosity reduces to the purely elastic membrane model. We assume that the initial biconcave shape with a large diameter of 7.8 μm is the unstressed (reference) shape for membrane force calculations (78).

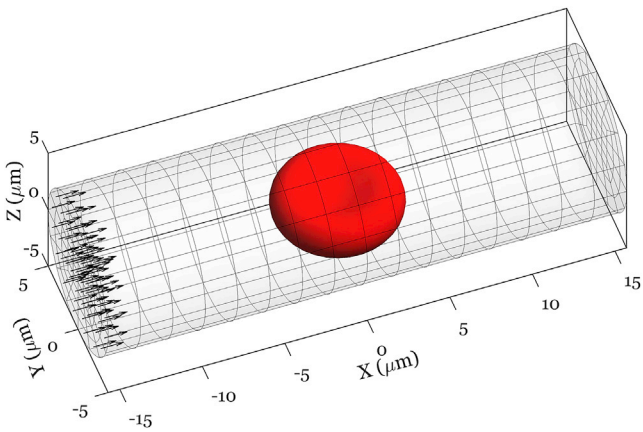

FIGURE 3 An RBC flow inside a straight cylindrical microcapillary with a 10 μm diameter under the influence of the pressure gradient of 4 mmHg/mm; the corresponding applied inlet pressure is 16.75 Pa (the microcapillary length equals the circumference) and the outlet is traction-free surface. No-slip boundary condition is applied to sidewalls. To see this figure in color, go online.

TABLE 1 The material properties of the cell membrane (15,34,76,77)

Elastic membrane properties	
E_S	5.3 μN/m
E_D	265 μN/m
E_B	0.2 nN·nm
Viscoelastic membrane properties	
μ_m	0–1 μN·s/m
$k' = 33.3\ E_S$	176.7 μN/m

Fluid flow inside the microcapillary is generated by imposing a constant pressure gradient of 4 mmHg/mm along the length of the microcapillary. Without loss of generality, we apply the inlet pressure of 16.75 Pa to the inlet surface and let the outlet be a traction-free surface. We assume a no-slip velocity condition on the sidewalls. The resulting fluid flow has a parabolic profile in the plane of the YZ axis in the absence of the RBC.

In this problem, the flow must be simulated over a considerable length of time to obtain the steady-state shape of the RBC. An approach is adopted to avoid the excessive computational effort associated with meshing the boundary of a long microcapillary. The RBC is placed in the middle of a relatively short microcapillary, whose length is chosen so that the boundary effects at the inlet and outlet are negligible near the middle. This approach consists of subtracting the rigid-body motion of the RBC in the X-direction from the total displacement of the RBC after each time increment. This is similar to observing the motion of the RBC from a reference point that moves along the microcapillary with the RBC.

Fig. 4 presents snapshots of the deformation of an RBC flowing in a straight microcapillary with increasing membrane viscosity. Experimental measurements of the RBC shape evolution during start-up flow (79) at the same time steps are provided to compare with the numerical results. What stands out in Fig. 4 is that the general deformation patterns of the RBC with the membrane viscoelasticity model resemble the experimental results. On the other hand, it can be seen that the purely elastic membrane model reaches the steady-state parachute shape very quickly. The change in the deformation of the purely elastic membrane model is insignificant after 0.05 s.

A closer inspection of Fig. 4 reveals that the pressure-driven parabolic flow field pushes the rear portion of the rim inward, creating an infolding bending. Consequently, this deformation redistributes the intracellular fluid toward the front side of the rim, creating a bulging-out bending. Initially, the biconcavity of the dimple portion of the red

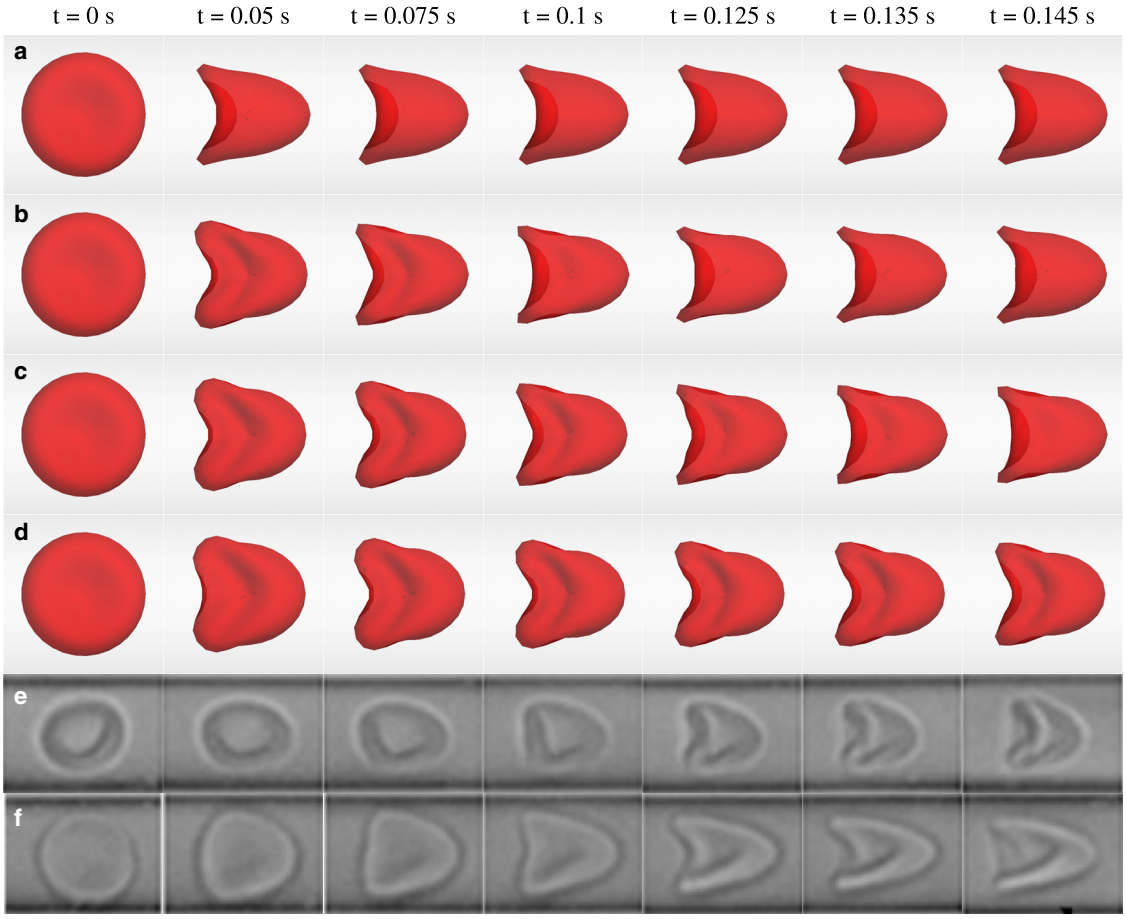

FIGURE 4 The snapshots of an RBC flow inside of a microcapillary with a 10 μm diameter (*a*) with purely elastic membrane, (*b*) with membrane viscosity of $\mu_m = 0.318$ μN·s/m, (*c*) with membrane viscosity of $\mu_m = 0.55$ μN·s/m, (*d*) with membrane viscosity of $\mu_m = 1$ μN·s/m. Experimental images in (*e*) and (*f*) are taken and reprinted with permission from (79). Copyright 2011, Elsevier. To see this figure in color, go online.

cell persists in its inward concavity, but slowly yields to intracellular fluid stresses. As the intracellular fluid is redistributed, it slowly flattens the inward concavity of the dimple portion and, with an increasing rate, pushes it outward in a snapping-like bending. This transition of the dimple portion from inward concavity to a flattened shape takes a longer time with a larger membrane viscosity. As the flattened dimple shape creates more room for intracellular fluid, the rear portion of the rim further bends inward, taking the shape of the parabolic flow field, and the front side of the rim further bulges out. This shape transition through membrane deformation and intracellular fluid flow leads to a parachute-like steady-state shape.

Next, we quantitatively analyze the magnitude and rate of RBC deformation. We use the extension parameter to describe the RBC shape evolution (79,80). The expression for the extension parameter (EX) has the form of $EX = \log_2[1/\widehat{a}(t)^2]$ with $\widehat{a}(t) = a(t)/a_0$ and $a(t)$ is the minimum of the eigenvalues of the ellipsoidal shape that has the same moment of inertia as the deformed RBC shape at time t and a_0 is its initial value for the biconcave shape (15,81–83). In a sense, the extension parameter describes how much the cross-sectional area of the RBC biconcave shape changes over time from the initial circular shape, which has the value of EX = 0. Fig. 5 compares the extension of an RBC as a function of time with increasing membrane viscosity, and the inset compares the numerical results with the experimental results (79) for initial timescale. The pressure gradient along the cylindrical microcapillary is 4.2 mmHg/mm in this case. The rate of deformation is higher in the purely elastic membrane model than in the model that includes viscoelasticity, and it decreases with increasing membrane viscosity. However, all models approach the same extension value over a long time span when the red cell reaches the steady-state parachute shape. The time required to reach the steady-state parachute shape increases with the membrane viscosity. As can be seen in the inset of Fig. 5, the numerical results with the membrane viscoelasticity model are in line with the microfluidic experimental results. The discrepancy in the initial value of the extension parameter is likely due to the fact that the initial shape of the RBC in the experiment is more similar to an ellipse than to a circle (79). Due to differences between the simulation and experimental setups as well as uncontrolled

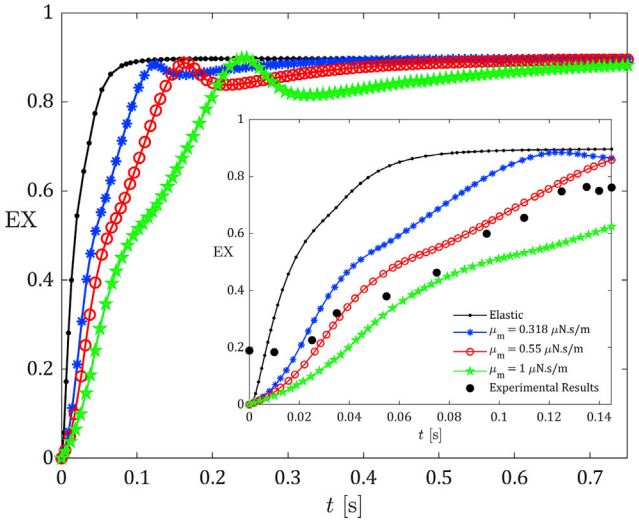

FIGURE 5 The extension parameter as a function of time for different values of membrane viscosity μ_m for an RBC flow in a straight microcapillary. The experimental results are taken from (79). To see this figure in color, go online.

factors in the experiments and image analysis, the comparisons between simulation and experimental results should not be considered as direct comparisons. We also remark that, in addition to including membrane viscosity, variations in some elastic properties of the membrane could also lead to closer agreements with the experimental results (see section S2 in the supporting material for details). Overall, the results here therefore only highlight membrane viscosity as a largely unexplored effect that could significantly impact the dynamics of an RBC flowing in a microcapillary, among other membrane properties.

Effects of viscosity ratio

Prior studies (16,29–31) that have noted the importance of the transient timescale of RBC dynamics have taken the approach of using higher intracellular fluid viscosity as a proxy for the effects of membrane viscoelasticity. The reason for using this approach, rather than modeling membrane viscoelasticity, is because of the ease of obtaining the solution using BIEs without the need to modify the mathematical formulation of membrane mechanics as shown in this paper. This approach only involves the use of higher values of λ; the viscosity ratio of intracellular fluid to extracellular fluid in Eqs. 2 and 3. From now on, we shall refer to this parameter λ as a viscosity ratio. Several reports have shown that the use of the higher viscosity ratio to describe the effects of membrane viscoelasticity captures the dynamics of RBC under shear flow in an unbounded domain qualitatively but not quantitatively (17,31). The rate of RBC deformation decreases with increasing viscosity ratio; however, the magnitude and rate of deformation differ using the membrane viscoelasticity model in an unbounded domain under a simple shear flow.

We investigated the effects of the high viscosity ratio on RBC deformation in a confined domain using the straight cylindrical microcapillary geometry shown in Fig. 3. We vary the viscosity ratio λ from 5 to 50, using the purely elastic membrane model with a pressure gradient of 4.2 mmHg/mm along the length of the microcapillary. Similarly to Fig. 5, Fig. 6 compares the extension of an RBC as a function of time with an increasing viscosity ratio, and the inset compares the numerical results with the experimental results for the initial timescale. The rate of deformation decreases with increasing viscosity ratio. However, all models approach the same extension value in a long time span and reach the steady-state parachute shape. The time required to reach the steady-state parachute shape is longer with increasing viscosity ratio. As can be seen in the inset, the numerical results with the higher viscosity ratio are in line with the experimental results, as opposed to the case with $\lambda = 5$.

Overall, these results illustrate similar effects of the viscosity ratio on RBC deformation to the membrane viscoelasticity in a confined domain. This finding broadly supports the work of previous numerical studies on the effects of membrane viscoelasticity on RBC dynamics in an unbounded domain under shear flow (17,31). However, the difference between the results in Figs. 5 and 6 is the quantitative effects such as the rate and magnitude of RBC deformation. In addition, there are significant differences in the mode of RBC deformation with the purely elastic membrane model with a higher viscosity ratio compared with the membrane viscoelasticity model. For example, snapping-like bending in the dimple region of the RBC is a characteristic feature of the RBC dynamics with the membrane viscoelasticity model, but this shape transition from the inward concavity to the flattened membrane of the dimple region

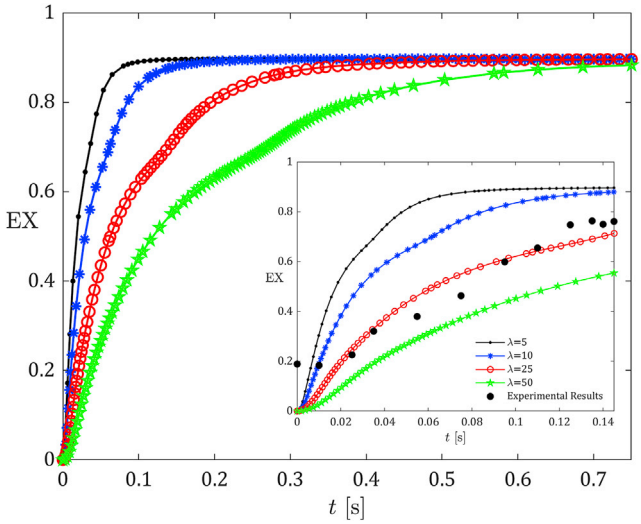

FIGURE 6 The extension parameter as function of time for different values of viscosity ratios λ for an RBC flow in a straight microcapillary. The experimental results are taken from (79). To see this figure in color, go online.

occurs smoothly in the case with a purely elastic membrane with higher viscosity ratio. In case of a higher intracellular fluid viscosity, the viscous dissipation effects are the main physical reason behind the lower deformation rate (16,84). Dissipation of the energy associated with the external parabolic flow field increases with higher intracellular fluid viscosity, which decreases the rate of deformation of the RBC membrane, even though the membrane does not do extra work in response to the external flow field, as in the case with the membrane viscoelasticity model. In a sense, the work associated with the redistribution of intracellular fluid within the cell membrane is the physics behind the decrease in the deformation rate. Thus, the results of the purely elastic membrane model with a high viscosity ratio need to be interpreted with caution, because it is possible that these results may underestimate the role of the membrane forces due to external hydrodynamical stresses. We conclude that the membrane viscoelasticity needs to be properly modeled to describe the complex shape transition of the RBC membrane and to have a better understanding of the transient RBC dynamics in a microcapillary, instead of mimicking its effects on the RBC deformation using the higher viscosity ratio.

Constricted microcapillary

RBCs often encounter variations in their geometrical confinement; for example, when entering or leaving small blood passages in the body (85,86). In particular, the cells need to deform significantly to squeeze through micrometer-sized slits in the spleen (87,88). The dynamics of RBCs through these constrictions has been linked to the removal of aging and diseased cells (89), ATP release (86,90–92), and volume regulation (93,94). For its physiological relevance, the dynamics of RBCs squeezing through constricted microcapillaries has received considerable attention (6,11,27,56,93,95,96). However, the effect of membrane viscoelasticity has been largely overlooked in previous studies. In this section, we examine how membrane viscoelasticity influences the motion and deformation of RBCs flowing through a microcapillary with a small constriction.

Similar to the case with a straight microcapillary, we consider the dynamics of an RBC flowing through a cylindrical, rigid, constricted microcapillary with a diameter of 10 μm at the inlet and outlet and a constriction diameter of 6 μm. An RBC with a 7.8 μm diameter is placed near the inlet surface. Fig. 7 shows the setup of the problem and the initial position and orientation of the RBC. The viscosity ratio is taken as $\lambda = 5$ in this section.

To study the effects of membrane viscosity on the deformation and motion of an RBC while flowing through a constriction, we varied the membrane viscosity from 0 to 1 μN.m/s. Fluid flow inside the microcapillary is generated by imposing a constant pressure gradient of 8 mmHg/mm

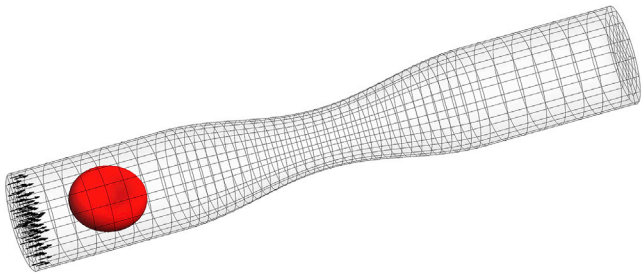

FIGURE 7 The problem statement of an RBC flow inside a cylindrical constricted microcapillary with a 10 μm inlet and outlet diameter and 6 μm constriction diameter under the influence of the pressure gradient of 8 mmHg/mm; the corresponding applied inlet pressure is 67 Pa (the microcapillary length equals twice the inlet circumference) and the outlet is a traction-free surface. No-slip boundary condition is applied to sidewalls. To see this figure in color, go online.

along the length of the microcapillary. Without loss of generality, we apply the inlet pressure of 67 Pa to the inlet surface and let the outlet be a traction-free surface. The resulting fluid flow has a parabolic profile in the cross section of the flow direction with increasing fluid velocity in the restricted region and consequently increased fluid shear stresses.

Fig. 8 presents snapshots at times $t = 0, 4, 8, 12, 16,$ and 20 ms of the motion and deformation of an RBC while squeezing through the constriction. The four panels in Fig. 8 correspond to increasing membrane viscosity values. There is a significant difference between the purely elastic membrane model and the viscoelastic membrane models. However, no significant differences are evident between the membrane viscosity values at this very short timescale. It is apparent that the RBC with a purely elastic membrane model squeezes through the constriction and travels faster. Furthermore, as shown in Fig. 9, the

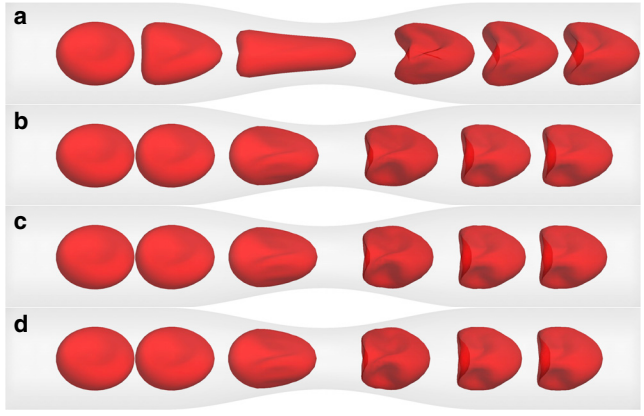

FIGURE 8 The snapshots of the motion and deformation of an RBC squeezing through a constriction with a 6 μm diameter (*a*) with purely elastic membrane, (*b*) with membrane viscosity of $\mu_m = 0.318$ μN·s/m, (*c*) with membrane viscosity of $\mu_m = 0.55$ μN·s/m, and (*d*) with membrane viscosity of $\mu_m = 1$ μN·s/m. Membrane profiles are taken at times $t = 0$, 4, 8, 12, 16, and 20 ms. To see this figure in color, go online.

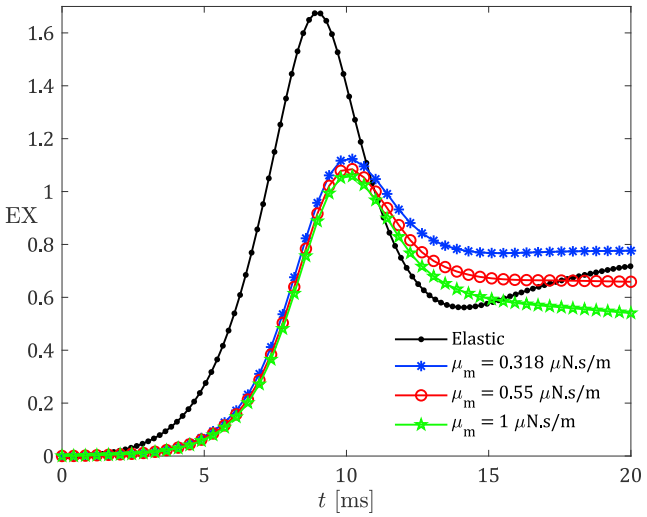

FIGURE 9 The extension parameter as a function of time for different values of membrane viscosity μ_m for an RBC flow in a constricted microcapillary. To see this figure in color, go online.

deformation is highest in the purely elastic membrane while squeezing through constriction compared with the membrane viscoelasticity models, where the membrane experiences the highest external fluid stresses.

The above findings point to the importance of accounting for membrane viscoelasticity in capturing the short-timescale dynamics of the RBC when squeezing through a constricted microcapillary. The result is particularly pertinent to the studies of mechanotransduction of RBCs, where the increased cell deformation and membrane tension in constricted environments have been posited to trigger the opening of mechanosensitive ion channels on the RBC membrane (55,92,93,97). To this end, the isotropic membrane tension is calculated using the average of the principal components of the in-plane membrane stress $\boldsymbol{\sigma}$ (98,99). Snapshots of the spatial distribution of the isotropic membrane tension of an RBC when squeezing through a constriction with various membrane viscosities are shown in Fig. 10. Similar to the conclusions on cell deformation, there are significant differences in the magnitude and distribution of isotropic membrane tension between the purely elastic membrane model and the viscoelastic membrane models; however, the results are not sensitive to specific values of the membrane viscosity.

Taken together, our work has illustrated how neglecting membrane viscoelasticity can lead to substantially different deformation and membrane tension distribution of an RBC when squeezing through a constriction. Since possible activation sites of ion channels in the cell membrane are correlated with high-tension regions (100–103), these findings suggest the important roles of membrane viscoelasticity in constructing accurate biophysical models for mechanotransduction of RBCs in subsequent works.

CONCLUSIONS

We set out to assess the significance of membrane viscosity on RBC dynamics under pressure-driven flow in microcapillaries. We studied the impact of the membrane viscosity on the long-time-scale deformation of the RBC in a rigid cylindrical straight microcapillary and on the short-time-scale motion and deformation of the RBC in a constricted microcapillary. We summarize our key findings as follows.

First, for the long-timescale behavior in a straight capillary, the steady-state parachute shape attained by the RBC is the same whether the membrane is modeled as elastic or viscoelastic. However, the membrane viscosity significantly increases the time it takes to attain this parachute shape. In particular, our viscoelastic membrane model suggests that a closer agreement with experimental measurements (79) of the RBC shape and the extension parameter in time can be obtained with a physiologically consistent value for membrane viscosity, compared with a purely elastic membrane model with the same elastic membrane properties.

Second, most current studies in the literature model the intracellular fluid with increased viscosity as a proxy for modeling membrane viscoelasticity, since this can be done without modifying the mathematical formulation. This proxy approach can be calibrated to track averaged quantities such as the membrane extension parameter with experimental measurements, but there are notable differences in the actual mechanics response, which are especially important for mechanotransduction. In particular, the membrane undergoes smooth deformation in the proxy approach versus a snapback-type response with modeling of the membrane viscosity.

Third, for short-timescale behavior in a constricted capillary, the deformation as the RBC squeezes through the constriction is significantly larger when the membrane is modeled as purely elastic. However, the transit time through the constriction depends substantially less on the membrane viscosity. We expect that differences in membrane stresses during transit play a significant role when considering membrane viscosity, which has implications for mechanotransduction (93).

In the current study, comparison with experimental measurements is limited by the small number of relevant microfluidic measurements. A recently developed technique (29) that tracks RBCs in a comoving frame in time-dependent flows promises to be valuable for comparing our computational findings more extensively with the experimental measurements. Notwithstanding the relatively limited experimental results to compare, this work offers valuable results that add to the growing body of research that indicated the impact of the membrane viscoelasticity of an RBC in an unbounded domain. Moreover, this work contributes additional evidence that suggests significant effects of membrane viscosity on the RBC dynamics under the

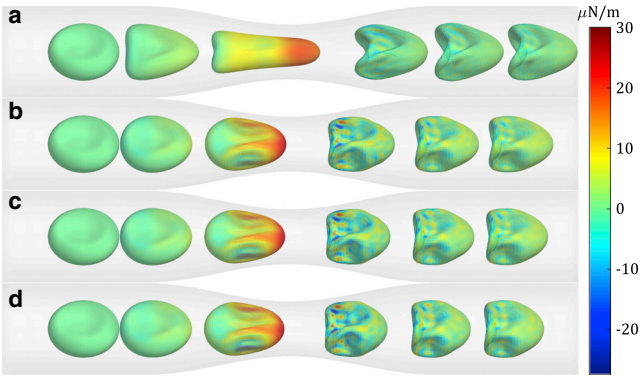

FIGURE 10 The snapshots of the isotropic membrane tension of an RBC squeezing through a constriction with a 6 μm diameter (*a*) with purely elastic membrane, (*b*) with membrane viscosity of $\mu_m = 0.318$ μN· s/m, (*c*) with membrane viscosity of $\mu_m = 0.55$ μN·s/m, and (*d*) with membrane viscosity of $\mu_m = 1$ μN·s/m. Membrane profiles are taken at times $t = 0$, 4, 8, 12, 16, and 20 ms. To see this figure in color, go online.

influence of pressure-driven flows in straight and constricted microcapillaries. It should be remarked that our findings here only suggest membrane viscoelasticity as a largely unexplored effect that could significantly impact the dynamics of RBC among other membrane properties. A more extensive parametric study is needed to examine the complex dependence of the RBC dynamics on different membrane properties, including, but not limited to, membrane viscosity.

Although the effects of the viscosity ratio on the RBC deformation are similar to the membrane viscoelasticity in a confined domain, one of the insights emerging from this study is that the physics behind the reduction of the rate and magnitude of RBC deformation with increasing viscosity ratio is due to the increasing amount of work associated with the redistribution of intracellular fluid within the cell membrane. However, the reduction in RBC deformation with increasing membrane viscosity is due to the viscoelastic membrane forces resisting the external flow field. An implication of this is the possibility that the results of the purely elastic membrane model with a high viscosity ratio may underestimate the role of the membrane forces. Thus, these findings have raised an important question that has a bearing on the activation mechanisms of mechanosensitive ion channels: How does the membrane viscosity affect membrane tension? More research is required to develop a deeper understanding of the role that membrane viscoelasticity plays in the development of membrane tension while flowing and squeezing through microcapillaries. This is important to study because the spatial distribution of the membrane tension depends on the rate of membrane deformation, the activation mechanisms of the mechanosensitive ion channels depend on the membrane tension, and, consequently, the feedback loop mechanisms that affect the RBC function and regulate its volume depend on the activation of the ion channels.

Furthermore, another natural progression of this work is to investigate the effects of membrane viscosity on recovery shape and time upon sudden arrest of the flow field after obtaining the steady-state parachute shape in a straight microcapillary (65,104) and upon egress from the constriction (11) to investigate the characteristic relaxation time of an RBC. Finally, the method developed in this study to investigate the RBC dynamics by incorporating the membrane viscoelasticity will be a valuable tool for the investigation of other interface problems, such as capsules, droplets, and swimmers in unbounded and confined domains.

SUPPORTING MATERIAL

Supporting material can be found online at https://doi.org/10.1016/j.bpj.2023.01.010.

AUTHOR CONTRIBUTIONS

A.G., M.V.S., and F.S. designed research. All authors performed the research and analyzed the data. All authors wrote, read, and approved the manuscript.

ACKNOWLEDGMENTS

O.S.P. was partially supported by the National Science Foundation under Grant No. 1830958.

DECLARATION OF INTERESTS

The authors declare no competing interests.

SUPPORTING CITATIONS

References (105–107) appear in the supporting material.

REFERENCES

1. Kang, Y. J., and S.-J. Lee. 2018. In vitro and ex vivo measurement of the biophysical properties of blood using microfluidic platforms and animal models. *Analyst.* 143:2723–2749.
2. Baskurt, O. K., M. R. Hardeman, and M. W. Rampling. 2007. Handbook of Hemorheology and Hemodynamics Volume 69. IOS Press.
3. Secomb, T. W. 2017. Blood flow in the microcirculation. *Annu. Rev. Fluid Mech.* 49:443–461.
4. Li, X., H. Li, H.-Y. Chang, …, G. Em Karniadakis. 2017. Computational biomechanics of human red blood cells in hematological disorders. *J. Biomech. Eng.* 139:0210081–02100813.
5. Farutin, A., and C. Misbah. 2014. Exact singularity subtraction from boundary integral equations in modeling vesicles and red blood cells. *Numer. Math. Theory Methods Appl.* 7:413–434.
6. Lu, H., and Z. Peng. 2019. Boundary integral simulations of a red blood cell squeezing through a submicron slit under prescribed inlet and outlet pressures. *Phys. Fluids.* 31:031902.
7. Peng, Z., R. J. Asaro, and Q. Zhu. 2011. Multiscale modelling of erythrocytes in Stokes flow. *J. Fluid Mech.* 686:299–337.
8. Hochmuth, R. M., and R. E. Waugh. 1987. Erythrocyte membrane elasticity and viscosity. *Annu. Rev. Physiol.* 49:209–219.

9. Hochmuth, R. M., P. R. Worthy, and E. A. Evans. 1979. Red cell extensional recovery and the determination of membrane viscosity. *Biophys. J.* 26:101–114.
10. Puig-de Morales-Marinkovic, M., K. T. Turner, …, S. Suresh. 2007. Viscoelasticity of the human red blood cell. *Am. J. Physiol. Cell Physiol.* 293:C597–C605.
11. Tomaiuolo, G., M. Barra, …, S. Guido. 2011. Microfluidics analysis of red blood cell membrane viscoelasticity. *Lab Chip.* 11:449–454.
12. Evans, E. A., and R. M. Hochmuth. 1976. Membrane viscoelasticity. *Biophys. J.* 16:1–11.
13. Rezghi, A., and J. Zhang. 2022. Tank-treading dynamics of red blood cells in shear flow: on the membrane viscosity rheology. *Biophys. J.* 121:3393–3410.
14. Guglietta, F., M. Behr, …, M. Sbragaglia. 2021. Loading and relaxation dynamics of a red blood cell. *Soft Matter.* 17:5978–5990.
15. Guglietta, F., M. Behr, …, M. Sbragaglia. 2020. On the effects of membrane viscosity on transient red blood cell dynamics. *Soft Matter.* 16:6191–6205.
16. Yazdani, A., and P. Bagchi. 2013. Influence of membrane viscosity on capsule dynamics in shear flow. *J. Fluid Mech.* 718:569–595.
17. Guglietta, F., M. Behr, …, M. Sbragaglia. 2021. Lattice Boltzmann simulations on the tumbling to tank-treading transition: effects of membrane viscosity. *Philos. Trans. A Math. Phys. Eng. Sci.* 379:20200395.
18. Gounley, J., and Y. Peng. 2015. Computational modeling of membrane viscosity of red blood cells. *Commun. Comput. Phys.* 17:1073–1087.
19. Gounley, J., G. Boedec, …, M. Leonetti. 2016. Influence of surface viscosity on droplets in shear flow. *J. Fluid Mech.* 791:464–494.
20. Rezghi, A., P. Li, and J. Zhang. 2022. Lateral migration of viscoelastic capsules in tube flow. *Phys. Fluids.* 34:011906.
21. Shi, X., S. Wang, and S. Zhang. 2013. Numerical simulation of the transient shape of the red blood cell in microcapillary flow. *J. Fluid Struct.* 36:174–183.
22. Barakat, J. M., and E. S. G. Shaqfeh. 2018. Stokes flow of vesicles in a circular tube. *J. Fluid Mech.* 851:606–635.
23. Barakat, J. M., and E. S. G. Shaqfeh. 2017. The steady motion of a closely fitting vesicle in a tube. *J. Fluid Mech.* 835:721–761.
24. Barakat, J. M., S. M. Ahmmed, …, E. S. G. Shaqfeh. 2019. Pressure-driven flow of a vesicle through a square microchannel. *J. Fluid Mech.* 861:447–483.
25. Pozrikidis, C. 2005. Numerical simulation of cell motion in tube flow. *Ann. Biomed. Eng.* 33:165–178.
26. Pozrikidis, C. 2005. Axisymmetric motion of a file of red blood cells through capillaries. *Phys. Fluids.* 17:031503.
27. Zhao, H., A. H. Isfahani, …, J. B. Freund. 2010. A spectral boundary integral method for flowing blood cells. *J. Comput. Phys.* 229:3726–3744.
28. Freund, J. B., and M. M. Orescanin. 2011. Cellular flow in a small blood vessel. *J. Fluid Mech.* 671:466–490.
29. Recktenwald, S. M., K. Graessel, …, C. Wagner. 2022. Red blood cell shape transitions and dynamics in time-dependent capillary flows. *Biophys. J.* 121:23–36.
30. Fischer, T. M., and R. Korzeniewski. 2015. Angle of inclination of tank-treading red cells: dependence on shear rate and suspending medium. *Biophys. J.* 108:1352–1360.
31. Li, P., and J. Zhang. 2021. Similar but distinct roles of membrane and interior fluid viscosities in capsule dynamics in shear flows. *Cardiovasc. Eng. Technol.* 12:232–249.
32. Pozrikidis, C. 1992. Boundary Integral and Singularity Methods for Linearized Viscous Flow. Cambridge University Press.
33. Barthès-Biesel, D. 2012. Microhydrodynamics and Complex Fluids. CRC Press.
34. Freund, J. B. 2014. Numerical simulation of flowing blood cells. *Annu. Rev. Fluid Mech.* 46:67–95.
35. Barthès-Biesel, D. 2016. Motion and deformation of elastic capsules and vesicles in flow. *Annu. Rev. Fluid Mech.* 48:25–52.
36. Pozrikidis, C. 2001. Interfacial dynamics for Stokes flow. *J. Comput. Phys.* 169:250–301.
37. Pozrikidis, C. 2003. Modeling and Simulation of Capsules and Biological Cells. CRC Press.
38. Pozrikidis, C. 2010. Computational Hydrodynamics of Capsules and Biological Cells. CRC Press.
39. Liu, Y., D. Zhang, and F. J. Rizzo. 1993. Nearly singular and hypersingular integrals in the boundary element method. *In* WIT Transactions on Modelling and Simulation WIT Press.
40. Liu, Y., and T. J. Rudolphi. 1991. Some identities for fundamental solutions and their applications to weakly-singular boundary element formulations. *Eng. Anal. Bound. Elem.* 8:301–311.
41. Liu, Y. 2000. On the simple-solution method and non-singular nature of the BIE/BEM — a review and some new results. *Eng. Anal. Bound. Elem.* 24:789–795.
42. Ganesh, M., and I. G. Graham. 2004. A high-order algorithm for obstacle scattering in three dimensions. *J. Comput. Phys.* 198:211–242.
43. Rahimian, A., S. K. Veerapaneni, …, G. Biros. 2015. Boundary integral method for the flow of vesicles with viscosity contrast in three dimensions. *J. Comput. Phys.* 298:766–786.
44. Beer, G., I. Smith, and C. Duenser. 2008. The Boundary Element Method with Programming: For Engineers and Scientists. Springer.
45. Gaul, L., M. Kögl, and M. Wagner. 2013. Boundary Element Methods for Engineers and Scientists: An Introductory Course with Advanced Topics. Springer Science & Business Media.
46. Pozrikidis, C. 2002. A Practical Guide to Boundary Element Methods with the Software Library BEMLIB. CRC Press.
47. Gürbüz, A. 2021. Simulations of Red Blood Cell Flow by Boundary Integral Methods. State University of New York at Buffalo, Ph.D. thesis.
48. Pozrikidis, C. 2003. Numerical simulation of the flow-induced deformation of red blood cells. *Ann. Biomed. Eng.* 31:1194–1205.
49. Vlahovska, P. M., T. Podgorski, and C. Misbah. 2009. Vesicles and red blood cells in flow: from individual dynamics to rheology. *C. R. Phys.* 10:775–789.
50. Li, H., and G. Lykotrafitis. 2014. Erythrocyte membrane model with explicit description of the lipid bilayer and the spectrin network. *Biophys. J.* 107:642–653.
51. Peng, Z., X. Li, …, S. Suresh. 2013. Lipid bilayer and cytoskeletal interactions in a red blood cell. *Proc. Natl. Acad. Sci. USA.* 110:13356–13361.
52. Namvar, A., A. J. Blanch, …, L. Tilley. 2020. Surface area-to-volume ratio, not cellular rigidity, determines red blood cell traversal through small capillaries. Preprint at bioRxiv. https://doi.org/10.1101/2020.07.11.191494.
53. Brody, J. P., Y. Han, …, M. Bitensky. 1995. Deformation and flow of red blood cells in a synthetic lattice: evidence for an active cytoskeleton. *Biophys. J.* 68:2224–2232.
54. Jay, A. W. 1975. Geometry of the human erythrocyte. I. Effect of albumin on cell geometry. *Biophys. J.* 15:205–222.
55. Peng, Z., O. S. Pak, …, Y.-N. Young. 2016. On the gating of mechanosensitive channels by fluid shear stress. *Acta Mech. Sin.* 32:1012–1022.
56. Li, J., G. Lykotrafitis, …, S. Suresh. 2007. Cytoskeletal dynamics of human erythrocyte. *Proc. Natl. Acad. Sci. USA.* 104:4937–4942.
57. Mahapatra, A., D. Saintillan, and P. Rangamani. 2020. Transport phenomena in fluid films with curvature elasticity. *J. Fluid Mech.* 905:A8.
58. Steigmann, D. J. 2017. The Role of Mechanics in the Study of Lipid Bilayers Volume 577. Springer.
59. Sauer, R. A., and T. X. Duong. 2017. On the theoretical foundations of thin solid and liquid shells. *Math. Mech. Solids.* 22:343–371.

60. Zarda, P. R., S. Chien, and R. Skalak. 1977. Elastic deformations of red blood cells. *J. Biomech.* 10:211–221.
61. Naghdi, P. M. 1973. The Theory of Shells and Plates. Springer, pp. 425–640.
62. Jenkins, J. T. 1977. The equations of mechanical equilibrium of a model membrane. *SIAM J. Appl. Math.* 32:755–764.
63. Tözeren, A., R. Skalak, …, S. Chien. 1982. Viscoelastic behavior of erythrocyte membrane. *Biophys. J.* 39:23–32.
64. Matteoli, P., F. Nicoud, and S. Mendez. 2021. Impact of the membrane viscosity on the tank-treading behavior of red blood cells. *Phys. Rev. Fluids.* 6:043602.
65. Prado, G., A. Farutin, …, L. Bureau. 2015. Viscoelastic transient of confined red blood cells. *Biophys. J.* 108:2126–2136.
66. Skalak, R., A. Tozeren, …, S. Chien. 1973. Strain energy function of red blood cell membranes. *Biophys. J.* 13:245–264.
67. Skalak, R. 1973. Modelling the mechanical behavior of red blood cells. *Biorheology.* 10:229–238.
68. Marques, S., and G. Creus. 2012. Computational Viscoelasticity. Springer Science & Business Media.
69. Simo, J., and T. Hughes. 2006. Computational Inelasticity Volume 7. Springer Science & Business Media.
70. Li, P., and J. Zhang. 2019. A finite difference method with subsampling for immersed boundary simulations of the capsule dynamics with viscoelastic membranes. *Int. J. Numer. Method. Biomed. Eng.* 35:e3200.
71. Li, P., and J. Zhang. 2020. Finite-difference and integral schemes for Maxwell viscous stress calculation in immersed boundary simulations of viscoelastic membranes. *Biomech. Model. Mechanobiol.* 19:2667–2681.
72. Helfrich, W. 1973. Elastic properties of lipid bilayers: theory and possible experiments. *Z. Naturforsch. C.* 28:693–703.
73. Guckenberger, A., and S. Gekle. 2017. Theory and algorithms to compute Helfrich bending forces: a review. *J. Phys. Condens. Matter.* 29:203001.
74. Jenkins, J. T. 1977. Static equilibrium configurations of a model red blood cell. *J. Math. Biol.* 4:149–169.
75. Chao, P.-C., A. Gürbüz, …, M. V. Sivaselvan. 2021. Fully implicit spectral boundary integral computation of red blood cell flow. *Phys. Fluids.* 33:071909.
76. Guido, S., and G. Tomaiuolo. 2009. Microconfined flow behavior of red blood cells in vitro. *C. R. Phys.* 10:751–763.
77. Tomaiuolo, G. 2014. Biomechanical properties of red blood cells in health and disease towards microfluidics. *Biomicrofluidics.* 8:051501.
78. Fischer, T. M., C. W. Haest, …, R. Skalak. 1981. The stress-free shape of the red blood cell membrane. *Biophys. J.* 34:409–422.
79. Tomaiuolo, G., and S. Guido. 2011. Start-up shape dynamics of red blood cells in microcapillary flow. *Microvasc. Res.* 82:35–41.
80. Dunn, G. A., and A. F. Brown. 1986. Alignment of fibroblasts on grooved surfaces described by a simple geometric transformation. *J. Cell Sci.* 83:313–340.
81. Krüger, T. 2012. Computer Simulation Study of Collective Phenomena in Dense Suspensions of Red Blood Cells under Shear. Springer Science & Business Media.
82. Krüger, T., F. Varnik, and D. Raabe. 2011. Efficient and accurate simulations of deformable particles immersed in a fluid using a combined immersed boundary lattice Boltzmann finite element method. *Comput. Math. Appl.* 61:3485–3505.
83. Ramanujan, S., and C. Pozrikidis. 1998. Deformation of liquid capsules enclosed by elastic membranes in simple shear flow: large deformations and the effect of fluid viscosities. *J. Fluid Mech.* 361:117–143.
84. Dasanna, A. K., J. Mauer, …, D. A. Fedosov. 2021. Importance of viscosity contrast for the motion of erythrocytes in microcapillaries. *Front. Phys.* 9
85. Sprague, R. S., M. L. Ellsworth, …, A. J. Lonigro. 1998. Deformation-induced ATP release from red blood cells requires CFTR activity. *Am. J. Physiol.* 275:H1726–H1732.
86. Wan, J., W. D. Ristenpart, and H. A. Stone. 2008. Dynamics of shear-induced ATP release from red blood cells. *Proc. Natl. Acad. Sci. USA.* 105:16432–16437.
87. Dao, M., I. MacDonald, and R. J. Asaro. 2021. Erythrocyte flow through the interendothelial slits of the splenic venous sinus. *Biomech. Model. Mechanobiol.* 20:2227–2245.
88. Gambhire, P., S. Atwell, …, A. Charrier. 2017. High aspect ratio submicrometer channels using wet etching: application to the dynamics of red blood cell transiting through biomimetic splenic slits. *Small.* 13:1700967.
89. Mebius, R. E., and G. Kraal. 2005. Structure and function of the spleen. *Nat. Rev. Immunol.* 5:606–616.
90. Forsyth, A. M., J. Wan, …, H. A. Stone. 2011. Multiscale approach to link red blood cell dynamics, shear viscosity, and ATP release. *Proc. Natl. Acad. Sci. USA.* 108:10986–10991.
91. Wan, J., A. M. Forsyth, and H. A. Stone. 2011. Red blood cell dynamics: from cell deformation to ATP release. *Integr. Biol.* 3:972–981.
92. Cinar, E., S. Zhou, …, J. Wan. 2015. Piezo1 regulates mechanotransductive release of ATP from human RBCs. *Proc. Natl. Acad. Sci. USA.* 112:11783–11788.
93. Danielczok, J. G., E. Terriac, …, L. Kaestner. 2017. Red blood cell passage of small capillaries is associated with transient Ca2+-mediated adaptations. *Front. Physiol.* 8:979.
94. Cahalan, S. M., V. Lukacs, …, A. Patapoutian. 2015. Piezo1 links mechanical forces to red blood cell volume. *Elife.* 4:e07370.
95. Ye, H., Z. Shen, …, Y. Li. 2021. Red blood cell hitchhiking enhances the accumulation of nano- and micro-particles in the constriction of a stenosed microvessel. *Soft Matter.* 17:40–56.
96. Faivre, M., C. Renoux, …, P. Connes. 2020. Mechanical signature of red blood cells flowing out of a microfluidic constriction is impacted by membrane elasticity, cell surface-to-volume ratio and diseases. *Front. Physiol.* 11:576.
97. Pak, O. S., Y.-N. Young, …, H. A. Stone. 2015. Gating of a mechanosensitive channel due to cellular flows. *Proc. Natl. Acad. Sci. USA.* 112:9822–9827.
98. Omori, T., T. Ishikawa, …, T. Yamaguchi. 2013. Membrane tension of red blood cells pairwisely interacting in simple shear flow. *J. Biomech.* 46:548–553.
99. Omori, T., T. Ishikawa, …, T. Yamaguchi. 2012. Tension of red blood cell membrane in simple shear flow. *Phys. Rev. E Stat. Nonlin. Soft Matter Phys.* 86:056321.
100. Sachs, F. 2018. Mechanical transduction and the dark energy of biology. *Biophys. J.* 114:3–9.
101. Murthy, S. E., A. E. Dubin, and A. Patapoutian. 2017. Piezos thrive under pressure: mechanically activated ion channels in health and disease. *Nat. Rev. Mol. Cell Biol.* 18:771–783.
102. Cox, C. D., C. Bae, …, B. Martinac. 2016. Removal of the mechanoprotective influence of the cytoskeleton reveals PIEZO1 is gated by bilayer tension. *Nat. Commun.* 7:10366.
103. Ranade, S. S., R. Syeda, and A. Patapoutian. 2015. Mechanically activated ion channels. *Neuron.* 87:1162–1179.
104. Wu, C., S. Wang, …, X. Li. 2021. Quantitative prediction of elongation deformation and shape relaxation of a red blood cell under tensile and shear stresses. *Phys. Fluids.* 33:111906.
105. Liu, Y. 2009. Fast Multipole Boundary Element Method: Theory and Applications in Engineering. Cambridge University Press.
106. Meiselman, H., and E. Evans. 1978. Membrane mechanical properties of ATP-depleted human erythrocytes. *Blood* 52:499–504.
107. Evans, J., W. Gratzer, …, K. Parker. 2008. Fluctuations of the Red Blood Cell Membrane: Relation to Mechanical Properties and Lack of ATP Dependence. *Biophys. J.* 94:4134–4144.